PERGAMON

International Journal of Heat and Mass Transfer 44 (2001) 1249–1257

International Journal of HEAT and MASS TRANSFER

www.elsevier.com/locate/ijhmt

Transitions of natural convection in a horizontal annulus

Jiro Mizushima *, Sachiko Hayashi, Takahiro Adachi [1]

Department of Mechanical Engineering, Doshisha University, 1-3 Tataramiyakotani, Kyotanabe, Kyoto 610-0321, Japan

Received 6 September 1999; received in revised form 31 March 2000

Abstract

Transitions of natural convection in an annulus between horizontal concentric cylinders are investigated theoretically by assuming two-dimensional and incompressible flow fields. It is assumed that the inner cylinder is kept at a higher temperature than the outer cylinder. It is confirmed by numerical simulations that dual stable steady solutions exist for Rayleigh numbers larger than a critical value. Bifurcation diagrams of the steady solutions are obtained by Newton–Raphson's method for various values of ratio of the inner cylinder diameter to the gap width and their linear stability is investigated. The origin of the dual solutions is clarified from the bifurcation analysis. © 2001 Elsevier Science Ltd. All rights reserved.

1. Introduction

Natural convection in an annulus between horizontal concentric cylinders is one of the most primitive models for heat exchangers. The convection always occurs when the inner cylinder is kept at a higher temperature than the outer cylinder even for very small magnitudes of temperature difference. The flow pattern of the convection is determined depending upon a set of parameters (A, Ra, Pr), where the aspect ratio A is the ratio of inner cylinder diameter D_i^* to the gap width L^* ($A \equiv D_i^*/L^*$), Ra is the Rayleigh number and Pr the Prandtl number.

Steady convection is attained at small values of the Rayleigh number irrespective of the values of A or Pr, whose flow pattern consists of two large circulations opposed symmetrically in both sides of the vertical center line of the circular annulus. The steady convection has been called as a crescent-shaped convection, which is characterized by an upward flow at the top region of the annulus. The flow and temperature fields of the crescent-shaped convection have been extensively investigated experimentally and numerically (for instance, see [1,2]).

The instability of the crescent-shaped convection of fluids with moderate values of the Prandtl number has been investigated extensively. Powe et al. [3] made experiments of the natural convection of air ($Pr = 0.7$) by visualizing flow patterns, and categorized the flow patterns obtained by their experiments and accumulated results by other researchers in a parameter space of (A, Ra). In the range of the aspect ratio $0 < A < 2.8$, the instability of the crescent-shaped convection induces an unsteady two-dimensional convection, which is characterized by oscillations about the longitudinal axis of the cylinders at the top region of the annulus. For $2.8 < A < 8.5$, an oscillatory convection exists above a critical Rayleigh number, which is characterized by a three-dimensional spiral motion in the upper portion of the annulus. For $A > 8.5$, two-dimensional multicellular convections appear as a result of instability of the crescent-shaped convection. This classification was confirmed by two-dimensional numerical simulations by Rao et al. [4].

Occurrences of dual steady solutions at Rayleigh numbers larger than a critical value were pointed out by Yoo [5], who made two-dimensional numerical simulations for air ($Pr = 0.7$) in the range of aspect ratio $0.1 \leqslant A \leqslant 10$. He observed dual steady solutions at $Ra > Ra_c \sim 3800$ for a small value of aspect ratio $A = 1.25$. The natural convection which appears at

* Corresponding author. Tel.: +81-774-65-6496; fax: +81-774-65-6835.

E-mail address: jmizushi@mail.doshisha.ac.jp (J. Mizushima).

[1] Present address: OTEC Laboratory, Faculty of Science and Engineering, Saga University, 1 Honjo-machi, Saga-shi, Saga, 840-8502, Japan.

0017-9310/01/$ - see front matter © 2001 Elsevier Science Ltd. All rights reserved.
PII: S0017-9310(00)00188-5

Nomenclature

A	aspect ratio of the inner cylinder diameter to gap width, D_i^*/L^*
D_i^*, D_o^*	diameters of inner and outer cylinders, respectively
g^*	acceleration due to gravity
L^*	gap width of the annulus, $(D_o^* - D_i^*)/2$
Pr	Prandtl number, ν^*/κ^*
Ra	Rayleigh number, $\gamma g \delta T^* L^{*3}/(\nu^*\kappa^*)$
Ra_S	Rayleigh number at the saddle-node bifurcation point
Ra_T	Rayleigh number at the virtual trans-critical bifurcation point
r	nondimensional radial coordinate
T	nondimensional temperature
$\tilde{T}_n, \tilde{\tilde{T}}_n$	modified nth order Chebyshev polynomials
T_i^*, T_o^*	temperatures at the inner and outer cylinders, respectively, $(\delta T^* = T_i^* - T_o^*)$
t	nondimensional time
u, v	nondimensional velocity components in the radial and azimuzal directions
u_1	radial velocity at $(r, \theta) = ((A+1)/2, 0)$

Greek symbols

γ^*	coefficient of thermal expansion
η	stretched coordinate in the radial direction
θ	azimuzal coordinate
κ^*	thermal diffusivity
λ_0	linear growth rate of the disturbance
ν^*	kinematic viscosity
Φ	solution of heat conduction equation for the motionless state
ϕ	nondimensional temperature deviation
ψ	nondimensional stream function

Subscripts

$\bar{}$	steady state solution
$'$	disturbance
$\hat{}$	Fourier coefficient of the disturbance

$Ra > Ra_c$ has a couple of counter-rotating vortices in the top region of the annulus and the direction of the flow is downward at the top of the annulus. We call this type of convection as a downward two vortex flow. It was found that the features of steady solutions for medium aspect ratios ($2.8 < A < 8.5$) are similar to those for large aspect ratios ($A > 8.5$). For $A = 10$, both types of convections are realized at $Ra > Ra_c \sim 1900$ and the crescent-shaped convection changes into a steady multicellular convection with two couples of vortices in the top region of the annulus when the Rayleigh number exceeds another critical value of about 3000, which is consistent with the results of Rao et al. [4]. We call this type of convection as an upward four vortex flow since the flow direction is upward at the top of the annulus.

Choi and Kim [6] studied the linear stability of the crescent-shaped convection of air ($Pr = 0.71$) by solving the linear equation for three-dimensional disturbances with a time marching method. It was shown that the principle of exchange of stabilities is valid for $A \geqslant 2.1$, which implies that the resultant three-dimensional spiral flow is not periodic in time for $A \geqslant 2.1$.

The linear stability theory for parallel flows was applied to the natural convection by Walton [7] and Dyko et al. [8], where an expansion in inverse powers of the aspect ratio A is employed. Dyko et al. [8] evaluated the critical Rayleigh numbers for the three-dimensional instability by using the linear stability theory and the energy method, and concluded that the instability is subcritical. However, the physical meaning of the 'instability' is unclear because there are two types of instabilities, explained by a subcritical pitchfork bifurcation and a trans-critical bifurcation, for such a case.

Thus, accumulated results on the pattern formation in a natural convection in a horizontal annulus revealed that the crescent-shaped convection changes into various types of convection depending upon the aspect ratio of the annulus as the Rayleigh number is increased. However, it is still unclear which kind of instability may induce the convection to change its shape with the increase or decrease of the Rayleigh number. In this paper, we will confirm the appearances of the convection patterns reported so far by two-dimensional numerical simulations and then seek the reason why the patterns are realized for a given set of parameters (A, Ra) by obtaining the whole bifurcation diagram of the solution branches for the steady natural convections with Newton–Raphson's iteration method. The stability of the steady state solution is analyzed by using the linear stability theory and the critical Rayleigh numbers for the appearance of different types of convections are evaluated from the bifurcation diagram. We assume that the fluid filled in the annulus is air with the Prandtl number being 0.7.

2. Mathematical formulation

Consider a convective motion of fluid confined in an annulus between horizontal concentric circular cylinders with the diameters of inner and outer cylinders D_i^* and D_o^*, respectively. Fig. 1 shows the geometry of the annulus and the coordinates system, where r^* is taken along the radial direction and θ is measured clockwise

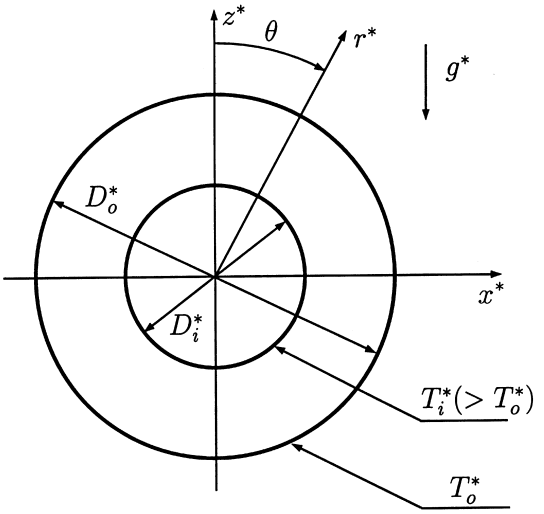

Fig. 1. Configuration and coordinates.

from the upward vertical plane through the center of cylinders. We represent physical quantities with its dimension by attaching a superscript * with it. The inner and outer cylinder surfaces are maintained at different uniform temperatures T_{i}^* and T_{o}^* respectively, where $T_{\mathrm{i}}^* > T_{\mathrm{o}}^*$ is assumed. We take the gap width $L^* = (D_{\mathrm{o}}^* - D_{\mathrm{i}}^*)/2$ as the representative length scale, L^{*2}/κ^* as the time scale, and $\delta T^* = T_{\mathrm{i}}^* - T_{\mathrm{o}}^*$ as the temperature scale to make all the physical quantities nondimensional.

We express the nondimensional temperature T of the fluid as a sum of the solution Φ of heat conduction equation for motionless state and its deviation ϕ as $T = \Phi + \phi$, where

$$\Phi = a \log r + b, \quad a = 1/\log\left(\frac{A}{A+2}\right),$$

$$b = -\log\left(\frac{A+2}{2}\right)\Big/\log\left(\frac{A}{A+2}\right).$$

We assume a two-dimensional flow field and adopt the Boussinesq approximation, then the dynamical equations for the stream function ψ and the temperature deviation ϕ are written in a nondimensional form as:

$$\frac{\partial \Delta\psi}{\partial t} - \frac{1}{r}J(\psi, \Delta\psi) = Pr\Delta^2\psi + \frac{1}{r}PrRa\frac{\partial\phi}{\partial\theta}\cos\theta + PrRa\left(\frac{\partial\phi}{\partial r} + \frac{a}{r}\right)\sin\theta, \tag{1}$$

$$\frac{\partial\phi}{\partial t} - \frac{1}{r}J(\psi,\phi) + \frac{a}{r^2}\frac{\partial\psi}{\partial\theta} = \Delta\phi, \tag{2}$$

where

$$J(f,g) = \frac{\partial(f,g)}{\partial(r,\theta)}, \quad \Delta = \frac{\partial^2}{\partial r^2} + \frac{1}{r}\frac{\partial}{\partial r} + \frac{1}{r^2}\frac{\partial^2}{\partial\theta^2}. \tag{3}$$

The flow field is characterized by three nondimensional parameters, i.e., the Rayleigh number $Ra \equiv \gamma^* g^* \delta T^* L^{*3}/(\kappa^* \nu^*)$, the Prandtl number $Pr \equiv \nu^*/\kappa^*$ and the aspect ratio $A \equiv D_{\mathrm{i}}^*/L^*$, where γ^*, κ^* and ν^* are the coefficients of thermal expansion, kinematic viscosity, thermal diffusivity of the fluid, respectively, and g^* is the acceleration due to the gravity.

The surfaces of inner and outer cylinders are assumed to be rigid and perfectly thermal conducting. Then, the boundary conditions are written as

$$\psi = \frac{\partial\psi}{\partial r} = 0, \quad \phi = 0, \quad \text{at } r = \frac{A}{2} \text{ and } \frac{A}{2} + 1 \tag{4}$$

and the periodic boundary condition is satisfied in the azimuzal direction for an arbitrary integer m so that

$$\psi(r,\theta) = \psi(r,\theta + 2m\pi), \quad \phi(r,\theta) = \phi(r,\theta + 2m\pi). \tag{5}$$

3. Numerical simulation of the dynamical equations

The dynamical equations (1) and (2) are solved numerically by using a finite difference approximation for the time derivative and expansions in terms of Chebyshev polynomials and Fourier functions for the r and θ dependences of ψ and ϕ.

For the convenience of numerical simulations, we transform the variable $r = [A/2, A/2+1]$ to $\eta = [-1, 1]$ by using the relation

$$\eta = 2(r - \tfrac{1}{2}(A+1)). \tag{6}$$

Then, we expand the stream function ψ and the temperature deviation ϕ by a series of Chebyshev polynomials and Fourier functions as

$$\psi(\eta,\theta,t) = \sum_{m=-M/2+1}^{M/2}\sum_{n=0}^{N} a_{mn}(t)\,\widetilde{\widetilde{T}}_n(\eta)\,\mathrm{e}^{\mathrm{i}m\theta},$$

$$\phi(\eta,\theta,t) = \sum_{m=-M/2+1}^{M/2}\sum_{n=0}^{N} b_{mn}(t)\,\widetilde{T}_n(\eta)\,\mathrm{e}^{\mathrm{i}m\theta}, \tag{7}$$

where the functions $\widetilde{T}_n(\eta)$ and $\widetilde{\widetilde{T}}_n(\eta)$ defined by

$$\widetilde{T}_n(\eta) = (1-\eta^2)T_n(\eta), \quad \widetilde{\widetilde{T}}_n(\eta) = (1-\eta^2)^2 T_n(\eta)$$

are the modified nth order Chebyshev polynomials which satisfy the boundary conditions (4) for ψ and ϕ, respectively. The coefficients $(a_{mn}(t), b_{mn}(t))^{\mathrm{T}}$ depend only on t. The integers M and N are the truncation parameters of the expansion.

Substituting Eq. (7) into Eqs. (1) and (2), and using the orthogonality of Fourier functions together with the collocation method in the η-direction, we obtain a set of ordinary differential equations for $a_{mn}(t)$ and $b_{mn}(t)$. The set of equations is solved by the finite difference method with a time increment Δt, where the Crank–Nicholson

scheme is used for the linear term, the Adams–Bashforth scheme for the nonlinear term, and the pseudo-spectrum method is utilized for the nonlinear term. The collocation points are taken as

$$\eta_i = \cos((i+1)\pi/(N+2)) \ (i = 0, 1, \ldots, 2N+1).$$

As for initial conditions, we adopt various kinds of flow and temperature fields, among which we choose two cases as typical examples expressed as initial condition A: $\mathrm{Re}(a_{mn}) = \mathrm{Im}(b_{mn}) = 0$, $\mathrm{Im}(a_{mn}) = \mathrm{Re}(b_{mn}) = 0.2$ for all (m,n), and initial condition B: $\mathrm{Re}(a_{mn}) = \mathrm{Im}(b_{mn}) = 0$, $\mathrm{Im}(a_{mn}) = \mathrm{Re}(b_{mn}) = -0.2$ for all (m,n). The direction of the flow is upward or downward at the top of the annulus in the initial conditions A and B, respectively.

We adopt a radial velocity u_1 at $(r,\theta) = ((A+1)/2, 0)$, the middle between the two circular cylinders in the top region of the annulus, as a representative quantity which characterizes the dynamical property of the nonlinear solutions. We have made numerical simulations for $A = 10$. The magnitude of the time step is taken as $\Delta t = 1.0 \times 10^{-3}$ and the truncation parameters are taken as $M = 64$, $N = 14$, which are confirmed being large enough by comparing results for various values of M and N.

We confirmed that the convection approaches to a steady state regardless of the initial condition for $Ra = 1800$, whose flow pattern is a crescent-shaped convection. The velocity u_1 approaches rapidly to a constant value of $u_1 = 0.846$ for both initial conditions A and B. On the other hand, the steady state solution for $Ra = 5000$ differs depending upon the initial condition. The velocity u_1 approaches to a constant value of $u_1 = 9.66$ for the initial condition A, whereas it attains to a different value of $u_1 = -12.77$ for the initial condition B, which are indicated by A and B in Fig. 2. The flow patterns of the steady state solutions attained from the initial conditions A and B are also depicted for their upper parts in Fig. 2. For the initial condition A, the flow pattern of the steady state solution consists of two couples of small vortices in the top region and two large circulations, which we call the upward four vortex flow. On the other hand, the flow field attained from the initial condition B consists of two small vortices in the top region and two large circulations, which we call the downward two vortex flow.

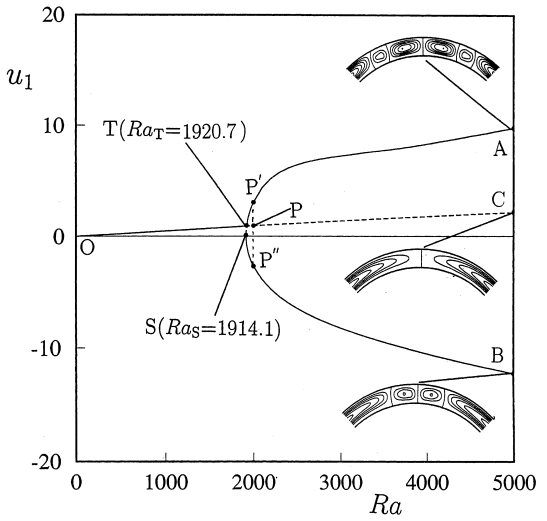

Fig. 2. Bifurcation diagram. $A = 10$. u_1: radial velocity at the center of the top of the annulus. Solid lines: stable steady state solutions. Dashed line: unstable steady state solution. S: saddle-node bifurcation point. T: virtual trans-critical bifurcation point.

4. Nonlinear steady state solution and the stability

The steady state equations for the steady state solution $(\bar{\psi}, \bar{\phi})$ are obtained by dropping the terms $\partial/\partial t$ in Eqs. (1) and (2). The boundary conditions in the radial direction for the steady solution $(\bar{\psi}, \bar{\phi})$ are the same with Eq. (4) for (ψ, ϕ), while we assume a symmetry condition $\bar{\psi}(r,\theta) = -\bar{\psi}(r,-\theta)$, $\bar{\phi}(r,\theta) = \bar{\phi}(r,-\theta)$ for $(\bar{\psi}, \bar{\phi})$ along the vertical center line of the annulus in place of the periodic condition (5) for (ψ, ϕ).

For numerical calculations of the steady state solution, we expand the solution $\bar{\psi}$ and $\bar{\phi}$ in a similar way to those for numerical simulations explained in the previous section. Substituting the expansion (7) into the steady state equations, and utilizing the collocation method, we obtain a set of algebraic equations for the coefficients a_{mn} and b_{mn}, where the collocation points are adopted as $\eta_i = \cos((i+1)\pi/(N+2))$ $(i = 0, 1, \ldots, N)$ and $\theta_i = (2i+1)\pi/2(M+1)$ $(i = 0, 1, \ldots, M)$ in a half of the whole region $(0 \leqslant \theta \leqslant \pi)$ by considering the symmetry. The set of algebraic equations for the coefficients is solved numerically by Newton–Raphson's method.

The stability of the nonlinear steady state solution is investigated by adding a disturbance to it and observing the time dependence of the disturbance. Thus, we express the stream function ψ and the temperature ϕ by the sum of the steady solution $(\bar{\psi}, \bar{\phi})$ and a disturbance (ψ', ϕ') as

$$\psi(r,\theta,t) = \bar{\psi}(r,\theta) + \psi'(r,\theta,t),$$
$$\phi(r,\theta,t) = \bar{\phi}(r,\theta) + \phi'(r,\theta,t).$$

The disturbance $(\psi'(x,z,t), \phi'(x,z,t))$ is assumed to have the time dependence expressed as $\psi'(r,\theta,t) = \hat{\psi}(r,\theta)\,\mathrm{e}^{\lambda_0 t}$ and $\phi'(r,\theta,t) = \hat{\phi}(r,\theta)\,\mathrm{e}^{\lambda_0 t}$, where λ_0 is complex in general and its real part $\mathrm{Re}[\lambda_0]$ shows the linear growth rate of the disturbance. If $\mathrm{Im}[\lambda_0] = 0$ when $\mathrm{Re}[\lambda_0]$ vanishes, it is said that an exchange of stabilities happens, and then the steady flow make a transition to another steady

state. Such a transition is classified into a pitchfork bifurcation, a saddle-node bifurcation or a trans-critical bifurcation by the bifurcation theory. If $\mathrm{Im}[\lambda_0] \neq 0$ when $\mathrm{Re}[\lambda_0]$ vanishes, the steady solution is unstable to an oscillatory disturbance and it make a transition to a periodic solution with the angular velocity $\mathrm{Im}[\lambda_0]$. Such a transition is called a Hopf bifurcation.

Substituting $\psi = \bar{\psi} + \psi'$ and $\phi = \bar{\phi} + \phi'$ into Eqs. (1) and (2), then subtracting the steady state equations from the resultant equations and dropping nonlinear terms of the disturbance $\hat{\psi}$ and $\hat{\phi}$, we obtain the following linearized equations for the disturbance

$$\lambda_0 \Delta\hat{\psi} = \frac{1}{r}\left\{J(\bar{\psi},\hat{\phi}) + J(\hat{\psi},\bar{\phi})\right\} + Pr\Delta^2\hat{\psi} + \frac{1}{r}PrRa\frac{\partial\hat{\phi}}{\partial\theta}\cos\theta + PrRa\frac{\partial\hat{\phi}}{\partial r}\sin\theta, \tag{8}$$

$$\lambda_0\hat{\phi} = \frac{1}{r}\left\{J(\bar{\psi},\hat{\phi}) + J(\hat{\psi},\bar{\phi})\right\} - \frac{a}{r^2}\frac{\partial\hat{\psi}}{\partial\theta} + \Delta\hat{\phi}. \tag{9}$$

The boundary conditions for the disturbances $(\hat{\psi},\hat{\phi})$ are the same with Eqs. (4) and (5) for (ψ,ϕ). The disturbance is decomposed into two modes according to the symmetry of the flow pattern along the vertical center line, which are symmetric (s)- and anti-symmetric (a)-modes, and the two modes can be treated separately.

As for numerical calculations of the linear growth rate, we expand the disturbance $\hat{\psi}$ and $\hat{\phi}$ in Fourier functions and Chebyshev polynomials as

$$\begin{aligned}\text{(s)-mode}: \quad \hat{\psi}(\eta,\theta) &= \sum_{m=0}^{M}\sum_{n=0}^{N} a_{mn}\widetilde{\widetilde{T}}_m(\eta)\sin\{(n+1)\theta\},\\ \hat{\phi}(\eta,\theta) &= \sum_{m=0}^{M}\sum_{n=0}^{N} b_{mn}\widetilde{T}_m(\eta)\cos(n\theta),\end{aligned} \tag{10}$$

$$\begin{aligned}\text{(a)-mode}: \quad \hat{\psi}(\eta,\theta) &= \sum_{m=0}^{M}\sum_{n=0}^{N} a_{mn}\widetilde{\widetilde{T}}_m(\eta)\cos(n\theta),\\ \hat{\phi}(\eta,\theta) &= \sum_{m=0}^{M}\sum_{n=0}^{N} b_{mn}\widetilde{T}_m(\eta)\sin\{(n+1)\theta\}\end{aligned} \tag{11}$$

for symmetric (s)- and anti-symmetric (a)-modes, respectively. Substituting the expansions (10) or (11) into Eqs. (8) and (9), and using the collocation method, we obtain a set of eigenvalue equations in a matrix form as

$$\mathbf{Aa} = \lambda_0\mathbf{Ba}. \tag{12}$$

where

$$\mathbf{a} = (a_{00}, a_{01}, \ldots, a_{2M+1,2N+1}, b_{00}, b_{01}, \ldots, b_{2M+1,2N+1})^{\mathrm{T}}$$

is a vector of $2\times(2M+2)\times(2N+2)$ and $\mathbf{A}$, $\mathbf{B}$ are matrices of $\{2\times(2M+2)\times(2N+2)\}\times\{2\times(2M+2)\times(2N+2)\}$. The eigenvalue λ_0 with a maximum real part determines the stability characteristics of the steady solution and the corresponding eigen vector represents the flow and temperature fields of the disturbance. The eigenvalue problem of the matrix is solved by a double QR method.

The steady state solutions and their growth rates are calculated for $1 \leqslant A \leqslant 20$ and $Ra \leqslant 5000$. All the numerical calculations are made with double precisions and the values of the truncation parameters in Eqs. (10) and (11) are taken as $M = 64$, $N = 14$. The numerical results are confirmed to be valid up to four significant digits by increasing the truncation parameters M and N up to $M = 128$ and $N = 28$.

Numerical simulations of dynamical equations have revealed that the solution approaches to one of the three steady states, i.e., the crescent-shaped convection, downward two vortex and upward four vortex flows, after enough time elapsed for $Ra < 5000$ depending on the initial condition and the Rayleigh number. We calculate the steady state solutions directly and obtain the whole bifurcation diagram of the solutions. As a representative quantity which characterizes the nonlinear steady state solution, we adopt the radial velocity u_1 at $(r,\theta) = ((A+1)/2, 0)$ also in this section.

The bifurcation diagram for $A = 10$ is shown in Fig. 2, where u_1 is depicted against Ra in the range of $0 \leqslant Ra \leqslant 5000$. The solid and dashed lines show the stable and unstable steady state solutions, respectively, in this figure. The line OTC indicates the crescent-shaped convection and the lines TA and TSB indicate the bifurcated flows. The solution on the bifurcated branch TA is the upward four vortex flow and the solution on TSB is the downward two vortex flow. It is apparently seen from this figure at first sight that the upward four vortex and downward two vortex flows bifurcate as a trans-critical bifurcation from the bifurcation point T. However, we will show later for the case of $A = 5$ that the trans-critical bifurcation inevitably becomes imperfect due to the inherent "imperfection" because of the curvature of the boundaries at the top region of the annulus, and that there are two continuous lines, OTA and CTSB. And the line OTC is discontinuous at T. The flow patterns of solution on each branch for $Ra = 5000$ are shown in Fig. 2, as typical examples.

The critical values of the Rayleigh numbers at the points indicated by S and T are evaluated as $Ra_{\mathrm{S}} = 1914.1$ and $Ra_{\mathrm{T}} = 1920.7$, respectively. The point S is a saddle-node bifurcation point or a turning point. And the point T is a virtual trans-critical bifurcation point though the bifurcation is imperfect. We have fitted the line OC and ASB in Fig. 2 with an straight line and a parabola, and determined the virtual trans-critical point by their intersection.

The bifurcation structure for $A = 10$ is summarized as follows. There is one steady state solution and the flow is the crescent-shaped convection for $Ra < Ra_{\mathrm{S}} = 1914.1$. As Ra increases, there appears two other steady state solutions at Ra_{S}, one of which, ST, is unstable and the other, SB, stable. As Ra increases further, the

number of the steady solution does not change at $Ra = Ra_T$, but the solution on the branch OC changes from the stable steady state solution to the unstable solution at the point T, and the branch STA changes from the unstable steady state solution to the stable solution. In this way, the stabilities of the two steady solutions on the branches OC and STA are exchanged at T. The explanation above is made by assuming that the trans-critical bifurcation is virtually perfect. However, the bifurcation is imperfect rigorously as noted before. Then, the bifurcation structure needs an alternative explanation. Thus, the bifurcation diagram of Fig. 2 is summarized as: there is a stable smooth transition branch OTA and there appear two branches at S, one of which, STC, is unstable and the other, SB, stable.

The line OTC indicates the crescent-shaped convection in Fig. 2. The linear stability of the crescent-shaped convection is investigated by solving Eqs. (8) and (9) under appropriate boundary conditions. It is found that the eigenvalue λ_0 is real, i.e., the exchange of stabilities is valid for $Ra \leqslant 5000$ and that the most unstable mode is the (s)-mode. The linear growth rate $\mathrm{Re}[\lambda_0]$ is depicted in Fig. 3. It is seen that the crescent-shaped convection is stable for $0 < Ra < Ra_T = 1920.7$, while it is unstable for $Ra > Ra_T$, which agrees with the result of the bifurcation analysis. The flow pattern of the disturbance at the point P ($Ra = 2000$) on the branch TC in Fig. 2 is depicted in Fig. 4.

The (s)-mode disturbance superposed on the crescent-shaped convection grows and saturates at a finite magnitude of the amplitude. Thus, the bifurcated solution is thought to consist of the crescent-shaped convection and the saturated disturbance. So, the most unstable mode of disturbance depicted in Fig. 4 may be compared with the difference of the bifurcated upward four vortex or downward two vortex flows from the

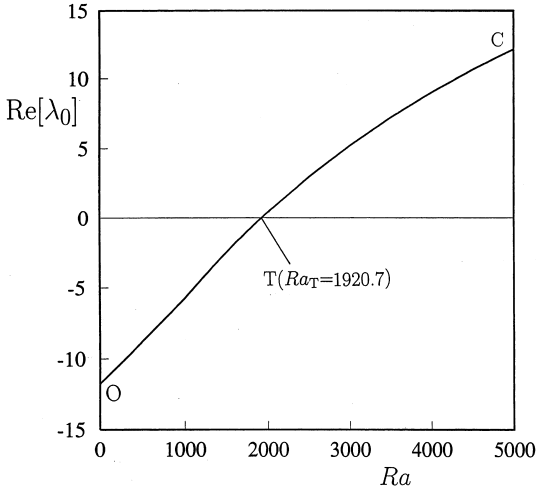

Fig. 3. Linear growth rate $\mathrm{Re}[\lambda_0]$. $A = 10$.

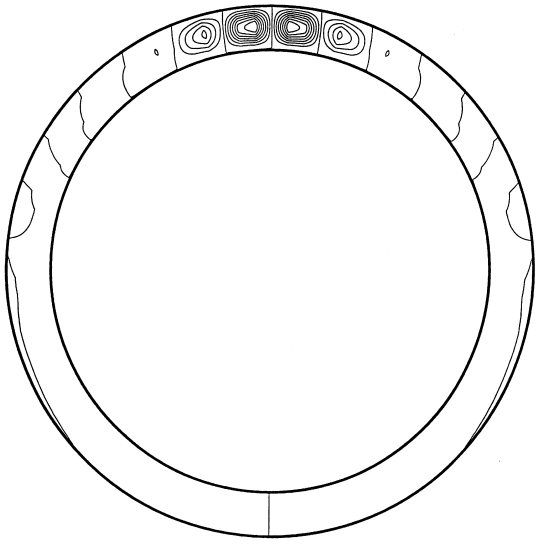

Fig. 4. Flow pattern of the disturbance. $Ra = 2000, A = 10$.

unstable crescent-shaped convection. The flow patterns of the difference of the steady state solutions from the crescent-shaped convection at the points P′ and P″ in Fig. 2 are calculated and compared with the disturbance shown in Fig. 4. The patterns of the three flow fields of the disturbances are too similar to be distinguished with each other, so we omit showing them to save space.

The bifurcation diagram for $A = 5$ constitutes of two lines OT′A and CT″SB as clearly seen in Fig. 5(a). The point indicated by S is a saddle-node bifurcation point in this figure, while the trans-critical bifurcation point cannot be defined exactly, so we have defined the points T′ and T″ as the nearest points between the lines OT′A and CT″SB. Fig. 5(b) is an enlargement of Fig. 5(a) in a neighbor of the points T′, T″. It is seen from Fig. 5(b) that the bifurcation is an imperfect trans-critical bifurcation. It is our conclusion that the bifurcation structure for $A = 10$ is also the imperfect trans-critical bifurcation as well as the case of $A = 5$ although the rigorous proof is cast to the weakly nonlinear stability theory. The bifurcation diagram for $A = 2$ is shown in Fig. 5(c). Only the saddle-node bifurcation point S is seen in Fig. 5(c) and the points T′ and T″ defined for the case of $A = 5$ cannot be well defined for $A = 2$.

We calculated the critical Rayleigh numbers Ra_S of the saddle-node bifurcation for various aspect ratios. The critical Rayleigh numbers Ra_S are tabulated in Table 1 and shown against A in Fig. 6 together with the critical value Ra_T of the virtual trans-critical bifurcation. The value Ra_T is evaluated by the intersecting point of the two lines, OC and ASB, where virtual lines OC and ASB indicate the basic crescent-shaped convection and bifurcated multicellular flows (see Fig. 5(a)).

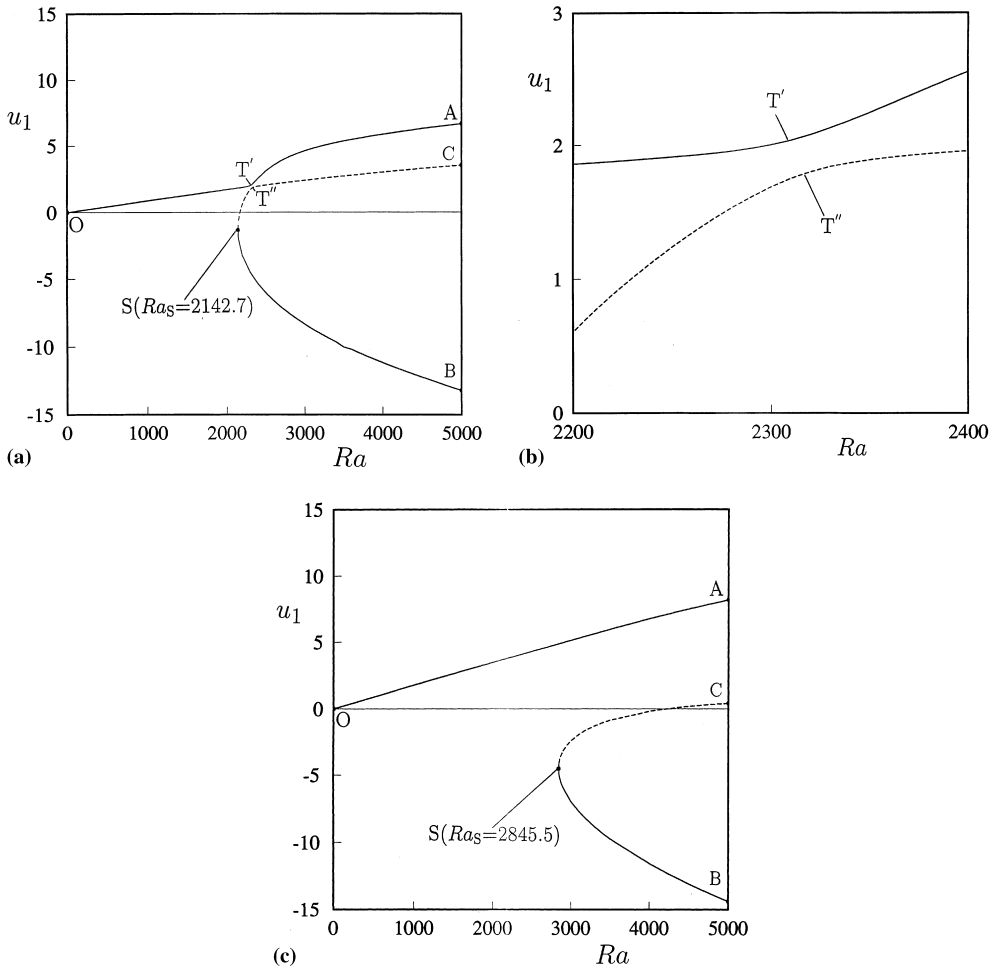

Fig. 5. Bifurcation diagrams. u_1: radial velocity at the center of the top of the annulus. S: saddle-node bifurcation point: (a) $A = 5$; (b) enlargement of figure (a), $A = 5$; (c) $A = 2$.

Table 1
Critical Rayleigh numbers Ra_S and Ra_T for various aspect ratios A

A	Ra_S	Ra_T
1	4471.6	–
2	2845.5	–
3	2434.5	–
4	2250.9	2837.0
5	2142.7	2312.0
6	2070.1	2158.0
10	1914.1	1921.0
20	1800.6	1800.0

The following asymptotic expressions for Ra_S and Ra_T are obtained for $A \gg 1$ from the numerical data of $A = 10$ and 20 in Table 1 by assuming an asymptotic form $c_1/(1 - c_2/A)$ with two constants c_1 and c_2:

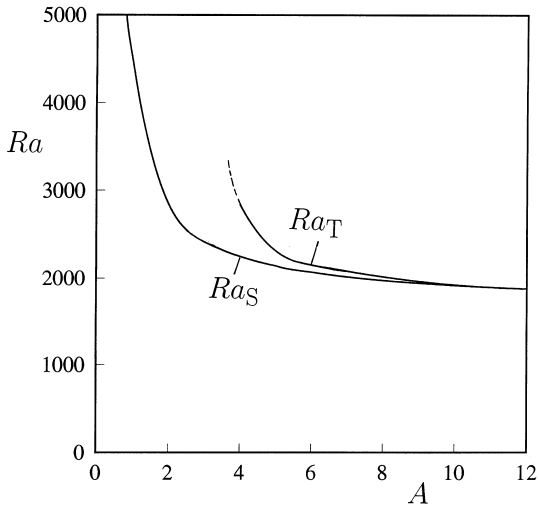

Fig. 6. Critical Rayleigh numbers Ra_S and Ra_T.

$$Ra_S = \frac{1699.5}{1-1.119/A} \sim 1699.5 + \frac{1901.7}{A},$$
$$Ra_T = \frac{1694.6}{1-1.177/A} \sim 1694.6 + \frac{1994.5}{A}. \quad (13)$$

The critical Rayleigh number obtained by Walton [7] is written as

$$Ra_c \sim 1707.8 + \frac{516.8}{A}. \quad (14)$$

In the above expressions (13), the asymptotic values of Ra_S and Ra_T tends to 1699.5 and 1694.6, respectively, as $A \to \infty$. These asymptotic values are in good agreement with the critical Rayleigh number $Ra_c = 1707.8$ for the Rayleigh–Bénard convection between two infinite parallel plates. Namely, it is thought that in the limit of $A \to \infty$ the bifurcation structure near $\theta = 0°$ approaches the pitchfork bifurcation as the case of the Rayleigh–Bénard convection. It is needless to say that the expression by Walton [7] coincides with the critical value of the Rayleigh-Bénard convection for $A \to \infty$ because his theory is based on the expansion by an inverse porwers of the aspect ratio from $A \to \infty$, i.e., the Rayleigh–Bénard problem. The critical Rayleigh number given in Eq. (14) should be compared with Ra_T where the crescent-shaped convection becomes unstable, and the expression (14) may be thought to give rather a good approximation for Ra_T in (13) if we consider the rough approximations assumed in Walton [7] though the coefficients of the term $1/A$ differ almost four times in magnitude between them. On the other hand, it is thought that the bifurcation structure near the equator ($\theta = 90°$) approaches to the property of the natural convection in an infinite vertical slot and the steady secondary flow occurs at the Grashof number $Gr \equiv Rs/Pr \sim 8000$ for the fluid with $Pr < 12.5$ (see [7]).

5. Discussion

There have been many reports for the transition of the natural convection in a horizontal annulus between two concentric cylinders. The most of them are numerical simulations, and their results have shown exchanges of flow patterns and multiple stable state solutions. The others are linear stability analyses based on the parallel flow assumption. The linear stability theory for parallel flows was shown to give a rather good approximate expression for the critical Rayleigh number Ra_T for large values of A. However, it cannot predict the imperfect trans-critical instability of the convection which has the inherent "imperfection" due to the curvature effect of the boundaries at the top region of the annulus. We have solved the full basic equations numerically and obtained the whole bifurcation structure of the steady state solutions regardless of their stability and clarified the meaning of the "instability" of the natural convection.

Yoo's results for the critical Rayleigh number above which multiple stable steady solutions exist are indicated by circles in Fig. 7, where the solid line shows our result for Ra_S. In fact, there are two stable and one unstable steady state solutions for $Ra > Ra_S$, so Yoo's results are in complete agreement with ours. The dotted lines show the transition lines proposed by Powe et al. [3]. The line AB shows the critical value of Ra where the natural convection becomes oscillatory keeping its two-dimensionality of the flow fields for $A < 2.8$. The crescent-shaped steady convection becomes three-dimensional spiral flows in the region above CD for $2.8 < A < 8.5$. The transition from the crescent-shaped convection to multi-cellular convections occurs at the critical Rayleigh number indicated by EF for $Ra > 8.5$. Transitions to oscillatory or chaotic convections are very interesting phenomena, and researches to clarify the root(s) to turbulent convections are in progress.

We have concluded that the bifurcation is an imperfect trans-critical bifurcation for every aspect ratio. The trans-critical bifurcation is imperfect even for very large values of aspect ratio such as $A = 10$, although the bifurcation diagram for $A = 10$ is seen at first sight to have a trans-critical bifurcation point T in Fig. 2. This is contrast to Taylor–Couette flow in a comparatively short annulus. The trans-critical bifurcation of the Taylor–Couette flow becomes imperfect for aspect ratios larger than a critical value, while it is perfect for smaller values of the aspect ratio [9]. The weakly nonlinear stability analysis may be helpful for a rigorous proof

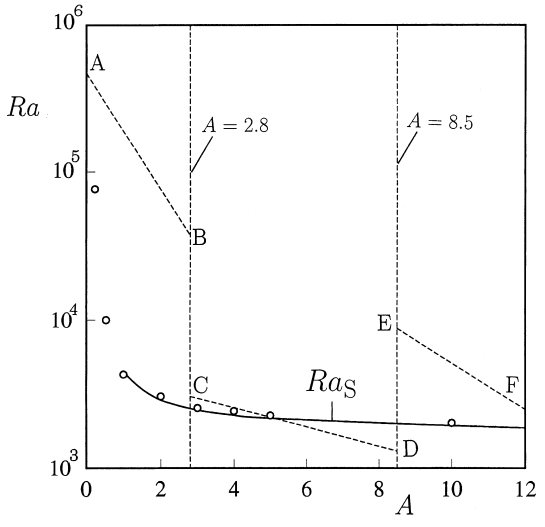

Fig. 7. Transition diagram. Circles: the critical Rayleigh numbers obtained by Yoo [5], above which multiple stable steady solutions exist. Dotted lines: transition lines proposed by Powe et al. [3].

that the bifurcation is imperfect. The imperfect trans-critical bifurcation is described by a single variable x as $dx/dt = \lambda_0 x + \lambda_1 x^2 + \lambda_2 x^3 + \lambda_3$. The bifurcation is imperfect if $\lambda_3 \neq 0$. It is noted that both the coefficients λ_1 and λ_3 vanish simultaneously as $A \to \infty$ for the natural convection in a horizontal annulus to yield the perfect pitchfork bifurcation as the case of the Rayleigh–Bénard convection. Then, the trans-critical and the saddle-node points, T and S, coincide.

Acknowledgements

The authors express their cordial thanks to Prof. M. Senda for valuable discussion. This work was partially supported by a Grant-in-Aid from the Ministry of Education, Science and Culture and also by Doshisha University's Research Promotion Funds.

References

[1] T.H. Kuehn, R.J. Goldstein, An experimental and theoretical study of natural convection in the annulus between horizontal concentric cylinders, J. Fluid Mech. 74 (1976) 695–719.

[2] Y.T. Tsui, B. Tremblay, On transient natural convection heat transfer in the annulus between concentric, horizontal cylinders with isothermal surfaces, Int. J. Heat Mass Transfer 27 (1984) 103–111.

[3] R.E. Powe, C.T. Carley, E.H. Bishop, Free convection flow patterns in cylindrical annuli, J. Heat Transfer 91 (1969) 310–314.

[4] Y.S. Rao, Y. Miki, K. Fukuda, Y. Tanaka, S. Hasegawa, Flow patterns of natural convection in horizontal cylindrical annuli, Int. J. Heat Mass Transfer 28 (1985) 705–714.

[5] J.S. Yoo, Dual steady solutions in natural convection between horizontal concentric cylinders, Int. J. Heat Fluid Flow 17 (1996) 587–593.

[6] J.Y. Choi, M.U. Kim, Three-dimensional liner stability of natural convective flow between concentric horizontal cylinders, Int. J. Heat Mass Transfer 36 (1993) 4173–4180.

[7] I.C. Walton, The stability of free convection in a horizontal cylindrical annulus, Quart. J. Mech. Appl. Math. 33 (1980) 125–139.

[8] M.K. Dyko, K. Vafai, A.K. Mojtabi, A numerical and experimental investigation of stability of natural convective flows within a horizontal annulus, J. Fluid Mech. 381 (1999) 27–61.

[9] K.A. Cliffe, Numerical calculations of the primary-flow exchange process in the Taylor problem, J. Fluid Mech. 197 (1988) 57–79.